Computational and Theoretical Chemistry 1107 (2017) 74–81

Contents lists available at ScienceDirect

Computational and Theoretical Chemistry

journal homepage: www.elsevier.com/locate/comptc

# Structure prediction of $(BaO)_n$ nanoclusters for $n \leqslant 24$ using an evolutionary algorithm

Susanne G.E.T. Escher, Tomas Lazauskas, Martijn A. Zwijnenburg, Scott M. Woodley *

*University College London, Department of Chemistry, 20 Gordon Street, London WC1H 0AJ, United Kingdom*

ARTICLE INFO

*Article history:*
Received 2 December 2016
Received in revised form 9 January 2017
Accepted 10 January 2017
Available online 12 January 2017

*Keywords:*
Inorganic nanoclusters
Global optimization
Evolutionary algorithm
Computational modelling
Barium oxide

ABSTRACT

Knowing the structure of nanoclusters is relevant to gaining insight into their properties for materials design. Computational studies predicting their structure should aim to reproduce experimental results. Here, barium oxide was chosen for its suitability for both computational structure prediction and experimental structure determination. An evolutionary algorithm implemented within the KLMC structure prediction package was employed to find the thermodynamically most stable structures of barium oxide nanoclusters $(BaO)_n$ with $n = 4 - 18$ and 24. Evolutionary algorithm runs were performed to locate local minima on the potential energy landscape defined using interatomic potentials, the structures of which were then refined using density functional theory. BaO clusters show greater preference than MgO for adopting cuts from its bulk phase, thus more closely resemble clusters of KF. $(BaO)_4$, $(BaO)_6$, $(BaO)_8$, $(BaO)_{10}$ and $(BaO)_{16}$ should be magic number clusters and each are at least 0.03 eV/BaO more stable than all other PBEsol local minima clusters found for the same size.


## 1. Introduction

Determination of the structure of materials is very important as their structure determines their properties. In particular, for nanoclusters it is difficult to determine the structure experimentally, so computational tools to achieve this become important. The structure of nanoclusters in particular is important as it allows for fine-tuning material properties for various applications—different properties such as colour, conductivity, and activity as catalysts, vary depending on the size and shape of the nanocluster.

Structure prediction is in principle a very difficult problem because it requires global optimisation of a function of many variables. The variables here are the atomic coordinates, and with clusters of many atoms, this becomes a problem which resides in a very high-dimensional space (for $N$ atoms, the space will be $3N - 6$-dimensional). There are several different approaches to tackling this problem; for details on different methods, multiple reviews of such methods are available [1–4]. In this study, the global optimisation method used is an evolutionary algorithm (EA) as implemented in KLMC (the Knowledge-led Master Code) [5,6] in combination with data-mining structures from other compounds.

In our calculations, evaluation (based on interatomic potentials (IPs)) and atomic structure relaxation for individual candidates in the EA runs was performed using routines within the GULP code [7], and then a selection of lowest-energy structures for each cluster size was used as input for density functional theory (DFT) calculations in FHI-aims [8]. Functionality within KLMC was also used to generate DFT input from the output of the EA/IP calculations and start FHI-aims runs automatically.

Here, barium oxide was chosen because it is particularly suited toward drawing a direct comparison between theory and experiment; it is simple enough to make the computational structure search tractable, but due to the high atomic number of barium cations, it is also possible to image the actual structure of BaO nanoclusters using experimental techniques such as transmission electron microscopy or scanning tunneling microscopy after deposition on a suitable surface. Corresponding experiments are planned in the near future, whereas computational results for $(BaO)_n$ nanoclusters are reported below. Structures of nanoclusters [9–11] have previously been resolved using microscopy techniques and in one case compared to computational results for size-selected metal clusters [12]. Hopefully this work will inspire further experiments that can generate data to compare to these computational predictions. All results reported here are of BaO clusters *in vacuo*; future work will also include a surface to match experimental conditions.

* Corresponding author.
*E-mail address:* Scott.Woodley@ucl.ac.uk (S.M. Woodley).

http://dx.doi.org/10.1016/j.comptc.2017.01.010
2210-271X/

## 2. Methods

### 2.1. Global Optimisation

The calculations were done in a two-step process.

In the first step, the primary approach used to explore each cluster size's potential energy landscape as efficiently as possible within a reasonable time (i.e. locating local minima (LM) by evaluating as few structures as possible) was that of an evolutionary algorithm implemented in the in-house software package, KLMC.

In EAs, concepts from natural selection are transferred to an application in order to find a solution that best fits the applied constraints. Here, solutions take the form of atomic coordinates, where the constraints are both the chosen energy function and composition of the cluster. A *population* of fixed size evolves over a number of *generations* which can be a fixed number or terminate on convergence. In KLMC, it is fixed, but post-processing scripts to ensure convergence are available. The EA here implements "crossover" by splicing in real-space parts of two structures within the current population to create a new structure, and "mutation" by Monte Carlo moves of atomic positions. Competition is simulated using tournaments to decide which structures survive from the new offspring and current candidates, and which current candidates become fathers (mothers are randomly chosen from the current population).

Additionally, in various steps of the KLMC implementation, there are checks to ensure that atoms are not too close to each other and that clusters are not fragmented. Too closely spaced atoms will cause repulsive forces which make a minimum in that region unlikely, and fragmented clusters will typically be higher in energy simply because there are less possible bonding interactions. Additionally, at the end of each EA generation, duplicates are removed via a graph theoretic comparison of structures.

For further details of the use of evolutionary algorithms in structure prediction, see the 2003 review by Johnston [2].

The top 20 structures found in the initial EA search were then inspected and used for higher accuracy local minimisations. For larger clusters, this was increased to top 40 structures which proved to be necessary as the global minimum (GM) did not appear in the top 20 structures in some cases — when there were many possible structures that are relatively close in energy, an IP which is parametrised for the bulk will struggle to get their energy ranking right (but will still predict where minima are located sufficiently well); for example it will too strongly penalise slightly polar structures even with shells. This pushed the PBESOL GM for some of the larger even-$n$ clusters out of the IP top 20.

The EA was generally run for a few hundred generations—100 were sufficient for cluster sizes of $n \leq 6$, but up to 1200 generations were necessary for convergence with larger-$n$ clusters.

### 2.2. Local optimisation: Step 1

For efficiency reasons, the energies of individual structures in the EA run and immediate relaxations were based on IPs. The accuracy of IP calculations is limited by the quality of the potentials (which in this case have been verified by running 3D periodic bulk simulations and comparing against several experimental results) [13]. The energies and LM's geometries from these are then used as a starting point for the next part of the calculation.

The IPs used in the calculations here were based on a Buckingham potential [14] taken from the in-house potential database [15] and were originally reported in a paper by Lewis and Catlow [16]. Within each EA iteration, this potential was first used with rigid ions to get a very rough and quick geometry that was close to an IP minimum before shells on oxygen atoms were included in the refinement.

### 2.3. Local optimisation: Step 2

To produce a more accurate potential energy surface, the top 20 structures for each cluster size were re-optimized using DFT. In all cases, geometry optimisations were performed using the FHI-aims electronic structure code and PBESOL GGA functional [17–19] with a tight basis set and first-tier basis functions, and then the 5 lowest energy structures for each cluster size with this energy function were re-optimized in the same basis set using a hybrid functional (PBESOL0) [20] to determine whether choice of density functional impacted the relative energies of different structures.

## 3. Results

The atomic structure of BaO nanoclusters was investigated here. The primary focus was on $(BaO)_n$ clusters with $n = 4$ and larger as $(BaO)_4$ is the smallest size where multiple LM were found. For comparison, the energy for $n = 1$ was also calculated, and $n = 2$ and 3 energies are included to extract second-order energy differences discussed in Section 3.4.

### 3.1. Structures of small $(BaO)_n$ clusters ($n \leq 12$)

As can be seen in Table 1, there exists only one stable structure for $n = 2$ and 3 clusters. For $n = 4$, the approximately cubic structure lies significantly lower in energy than the ring structure; previous studies have shown that this tends to be the case for metal oxides that display the rocksalt structure in the bulk [5]. Although the $n = 1$ stick and $n = 2$ and 4 ring configurations can be cut from the cubic rock salt structure, i.e. from the bulk phase for BaO, the $n = 4$ cuboid is the smallest cut that has no one or two coordinated atoms. We will refer to this cuboid configuration as a secondary building unit (SBU), which is itself composed of $2 \times 2 \times 2$ atoms.

**Table 1**
Lowest PBESOL energy minima structures of $(BaO)_n$ clusters for $n = 2 - 5$.

| | 1st | 2nd | 3rd |
|---|---|---|---|
| $n$ | | **2** | |
| |  | | |
| $\Delta E$/eV | 0.0 | | |
| $n$ | | **3** | |
| |  | | |
| $\Delta E$/eV | 0.0 | | |
| $n$ | | **4** | |
| |  |  | |
| $\Delta E$/eV | 0.0 | 2.999 | |
| $n$ | | **5** | |
| | 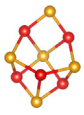 |  |  |
| $\Delta E$/eV | 0.0 | 0.010 | 0.052 |

**Table 2**
Three lowest PBESOL energy minima structures of $(BaO)_n$ clusters for $n = 6 - 12$.

| | 1st | 2nd | 3rd |
|---|---|---|---|
| $n$ | | **6** | |
| |  |  |  |
| $\Delta E$/eV | 0.0 | 0.134 | 0.666 |
| $n$ | | **7** | |
| | 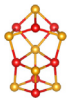 |  | 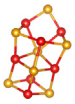 |
| $\Delta E$/eV | 0.0 | 0.007 | 0.113 |
| $n$ | | **8** | |
| |  |  | 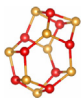 |
| $\Delta E$/eV | 0.0 | 0.284 | 0.587 |
| $n$ | | **9** | |
| |  |  |  |
| $\Delta E$/eV | 0.0 | 0.076 | 0.165 |
| $n$ | | **10** | |
| | 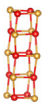 | 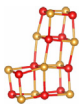 |  |
| $\Delta E$/eV | 0.0 | 0.393 | 0.585 |
| $n$ | | **11** | |
| |  |  |  |
| $\Delta E$/eV | 0.0 | 0.132 | 0.193 |
| $n$ | | **12** | |
| |  |  |  |
| $\Delta E$/eV | 0.0 | 0.047 | 0.347 |

**Table 3**
Three lowest PBESOL energy minima structures of $(BaO)_n$ clusters for $n = 13 - 18$ and $n = 24$.

| | 1st | 2nd | 3rd |
|---|---|---|---|
| $n$ | | **13** | |
| |  |  |  |
| $\Delta E$/eV | 0.0 | 0.114 | 0.173 |
| $n$ | | **14** | |
| |  |  |  |
| $\Delta E$/eV | 0.0 | 0.061 | 0.125 |
| $n$ | | **15** | |
| |  | 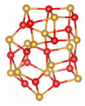 |  |
| $\Delta E$/eV | 0.0 | 0.241 | 0.242 |
| $n$ | | **16** | |
| |  |  |  |
| $\Delta E$/eV | 0.0 | 0.548 | 0.753 |
| $n$ | | **17** | |
| |  | 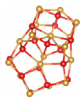 | 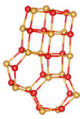 |
| $\Delta E$/eV | 0.0 | 0.204 | 0.398 |
| $n$ | | **18** | |
| | 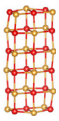 |  |  |
| $\Delta E$/eV | 0.0 | 0.108 | 0.374 |
| $n$ | | **24** | |
| |  |  |  |
| $\Delta E$/eV | 0.0 | 0.001 | 0.189 |

For $n = 5$, a number of higher-coordination structures are again found to be preferred over the ring configuration, which is not even ranked in the top 3.

As the size of clusters increases, so does the number of different LM structures. Table 2 shows only the three lowest energy structures for $(BaO)_n$ clusters with $n = 6 - 12$. For $n = 6$, the first instance where the GM for BaO clusters is different from that of MgO occurs: The lowest energy structure is another rocksalt-like structure, formed of $3 \times 2 \times 2$ atoms, or by merging 2 SBU, rather than the hexagonal prism, or barrel configuration. A similar result is found for KF; the energy difference between these two types of LM configurations is 0.134 eV for BaO compared to 0.167 eV for KF [5]. In contrast, MgO nanoclusters with $n = 6$ prefer the barrel shape LM.

More generally, the lowest energy structures resemble bulk cuts for all $n$ where it is possible to construct the configuration by merging $n = 4$ SBU, i.e. for even $n$, as well as $n = 9$. Again, our better LM for BaO match those for KF. In the case of $n = 7$, two very similar structures are thermally accessible at room temperature, while a large fragment of the lowest energy structure for $n = 11$ also resembles a cut from the bulk.

### 3.2. Structures of larger $(BaO)_n$ clusters ($n = 13 - 18$ and $n = 24$)

Table 3 shows the three lowest energy structures for $(BaO)_n$ nanoclusters with $n = 13 - 18$ and 24. For even-$n$, the lowest

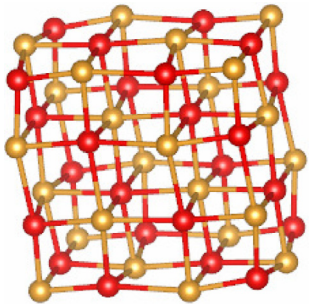

**Fig. 1.** The bulk cut structure for $(BaO)_{24}$ which is the GM as predicted by PBESOL0 calculations, and different from the GM found by GGA calculations.

energy structure is in every case a bulk cut, except for $n = 24$. In the case of $n = 18$, the cuboid bulk cut which might be naively hypothesized to be the lowest energy because its surface area is the lowest (composed of $4 \times 3 \times 3$ atoms) is actually shown to be significantly higher in energy than the cut of $6 \times 3 \times 2$-atoms. This can potentially be explained because the latter is much less polar (1.7 mD compared to 7.0 D). The large dipole moment is in line with results for the same cut in the case of MgO [21], which was found to have an even larger dipole moment of 17 D. The smaller value in BaO is most likely due to the higher polarizability of the barium cations. The large dipole moment for this structure, as well as the $n = 9$ bulk cut, is due to two faces of the cuboid having an odd number of atoms and are oppositely charged.

For odd $n$, the top 3 structures typically contain a bulk-like fragment, combined with some other structural elements such as barrels (see, for example, the third configuration for $n = 17$), as forming a bulk cut would lead to at least two atoms with a coordination of two.

Note that in the case of $n = 24$, using a hybrid functional (PBESOL0) to calculate the energies of different structures yields a qualitatively different picture: the hybrid functional predicts the $4 \times 4 \times 3$ bulk cut (see Fig. 1) to be the most stable in this case. For all other cluster sizes our tentative GM were not sensitive to choice of functional. All $n = 24$ GGA LM shown in Table 3 have a total of 91 bonds (iteratomic distance less than $\sim 2.96$ Å[1]); this is compared to 104 bonds in the $4 \times 4 \times 3$ bulk cut.

### 3.3. Density of local minima and size stability

To ascertain the stability of our tentative GM we produced Fig. 2. Considering each size, $n$, independently, we can expect, assuming a Boltzmann distribution, that the likelihood of nature adopting a particular LM configuration will be dependent upon the temperature and the energy difference from the global minimum. Thus, we show a "density of states" plot; number of local minima as a function of energy per BaO from the global minimum. In addition, we have marked the energy per BaO for the GM of the next smallest cluster—assuming a bath of $n = 1$ units, LM to the right (left) of this mark are more likely to fragment to (grow from) the smaller sized global minimum. The further the $n - 1$ mark is to the right, the more stable the size $n$ GM is to fragmenting into an $n$-1 cluster and an $n = 1$ unit. In this respect $n = 8$ is the most stable of the GM sizes examined in Fig. 2, followed by $n = 10$, 12, and 16. Note that only the lowest 20 energy LM found for each size are reported; structures too far to the right are unlikely to be adopted, and the number of these increase rapidly with $n$.

[1] The cutoff value came to be because some Ba—O bonds have a bond length slightly above 2.9 Å, while some Ba—Ba and O—O bonds have a bond length slightly below 3 Å, so this consistently avoids cation-cation and anion-anion bonds while picking up all anion-cation bonds.

When comparing the LM for size $n$ to the global minimum for $n - 1$ (green dashed lines in Fig. 2), all clusters of size $n > 8$ have 5 or less LM that are relatively more stable than the $n - 1$ GM. Typically, there are more LM to the left of the $n - 1$ GM mark if $n$ is an even number, and remarkably, in the case of $n = 17$, not a single structure is lower in energy (per formula unit) than the GM for $n = 16$. Moreover, looking at, for example, $n = 10$, two bulk cuts lie on the left hand side of the $n = 9$ GM mark, whereas the third best $n = 10$ LM, which also contains hexagonal rings (as well as the tetragonal rings found in the bulk rock salt phase), is found to the right of it. The sizes where only the respective GM is more stable than a smaller cluster are the ones with $n$ of 11, 14, 15 and 18; as mentioned above, the $n = 17$ clusters are unlikely to form due to $n = 16$ being lower in energy.

For odd $n$, where bulk cuts are not as markedly favoured, there tend to be a few more structures close to the global minimum. Generally, this number increases with increasing $n$. More importantly, there are a number of examples where there is only one structure for a particular size which is thermally accessible (the GM is much lower in energy than the second ranked LM of that size) and more stable than the $n - 1$ GM. These would be good target structures to try and synthesize. Good examples include $n = 8, 10$, and 16, all of which are bulk cuts. For $n = 9, 12, 14$ and 24 it is very unlikely to be able to synthesize just one type of configuration.

### 3.4. Second-order energies and structural motifs

In Fig. 3, energies relative to the nearest neighbours, the so-called second order energy differences, are shown:

$$\Delta E = E(n) - \frac{1}{2}(E(n+1) + E(n-1))$$

Negative energies correspond to clusters that are relatively more stable than extrapolation from clusters with 1 more and 1 less formula units; positive numbers correspond to less stable clusters. All clusters with negative second order energies resemble the bulk (rocksalt) structure; most of them have even $n$. The local minima in Fig. 3 also mark magic number sizes $n = m_i$, where the GM for $n = m_i$ is relatively more stable than the GM for $n = m_i + 1$ and $m_i - 1$. When clusters are created via laser ablation of a surface, and the resulting clusters measured in a mass spectrometer, then the larger peaks are expected for magic size numbers [22,23]. Magic numbers have also been predicted for $(NaCl)_nCl^-$, see [24]. A similar pattern is seen in Fig. 3.

This pattern is mirrored in a number of properties. The first is dipole moment, as shown in Fig. 4.

In most cases, structures with odd $n$ have dipole moments on the order of $\sim 1 - 10$ D, while the remaining structures have a few orders of magnitude lower (i.e. negligible) dipole moments. Notable data points are $n = 9$, which is the only polar cuboid bulk cut within this data set (and has 9-atom faces similar to the $4 \times 3 \times 3$ $(BaO)_{18}$ isomer discussed previously, which causes the dipole moment), and the two that follow the trend less $n = 13$ and 14. In the case of $n = 13$, most of the structure is arranged in close to (but not perfect) 3-fold symmetry along multiple axes, which probably contributes to reducing dipole moment. For $n = 14$, the lowest energy structure is not cuboid as with the other even-$n$ clusters presented here, and therefore does not have the same benefit of reducing polarity. The cuboid bulk cut that is possible ($7 \times 2 \times 2$ atoms) was found to be higher in energy (less stable). Referring back to Fig. 2, it is also notable that $n = 14$ has a GM much closer to the $n - 1$ GM than most other even-$n$ structures, further supporting the suggestion that dipole moments play a strong role in the relative stabilities of these structures.

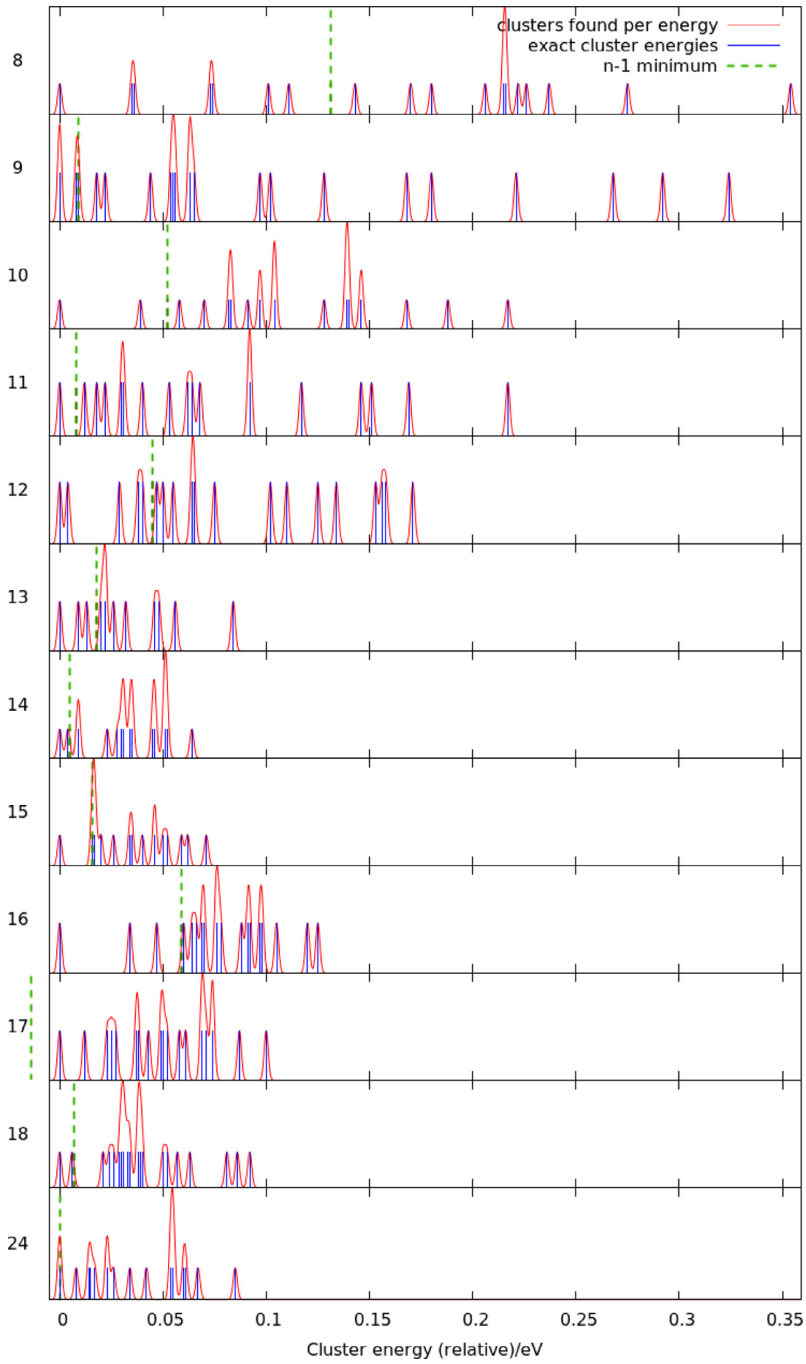


**Fig. 2.** Smeared density of states for different structures' PBESOL energies per formula unit, cluster sizes $n = 8 - 18$ and 24. Green dashed lines indicate the energy of the GM for $n - 1$-sized clusters.

The other property which reflects the energetic difference between even-$n$ and odd-$n$ structures is coordination number. BaO adopts the rocksalt structure, the average coordination number should typically increase with $n$ and approach a coordination of six asymptotically.

In Fig. 5, the odd $n$/even $n$ trend also shows for most clusters in that even-$n$ clusters tend to have higher coordination numbers relative to their neighbours; the only case where this doesn't hold is $n = 9$, which is also a bulk cut. With these generally energetically preferred, the assumption that BaO tends toward a high coordination number is confirmed; however for these sizes an asymptotic approach toward 6 is not yet visible as most of the atoms in these clusters will still be surface atoms which cannot have a full coordination shell. Note that the largest cluster size consider has an average coordination of around 4, whereas surface atoms can have a maximum coordination of 5 (e.g. perfect (001) surface).

### 3.5. Convergence of the evolutionary algorithm

An external KLMC Python script [25] has been used to analyse the convergence of the evolutionary algorithm in KLMC. The result for one run employed to search the IP landscape for $n = 15$ LM structures is shown in Fig. 6.

$n = 15$ was chosen because at that size range, the total number of structures found will far exceed the number of "LM structures" shown in previous figures and tables.

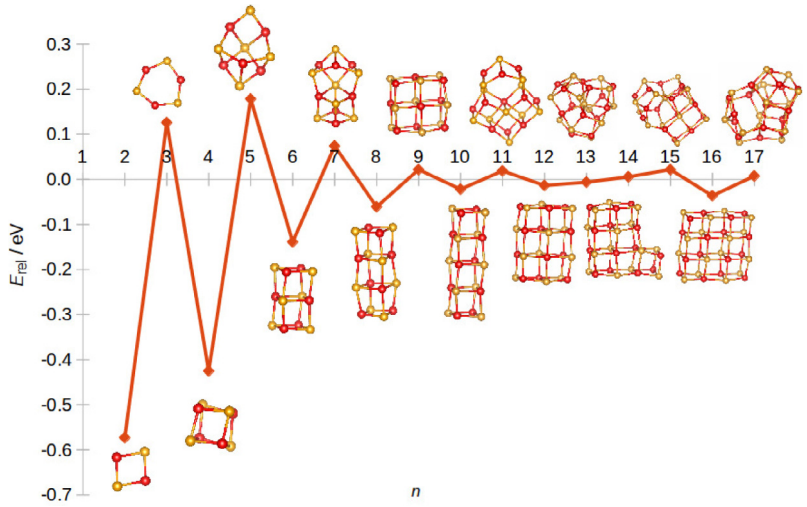


**Fig. 3.** Second-order energy differences of $(BaO)_n$ clusters for $n = 2 - 17$. Energies calculated with the PBESOL functional.

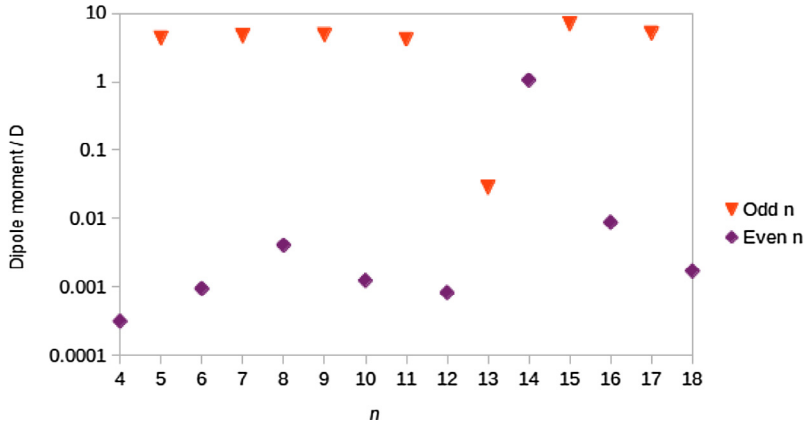


**Fig. 4.** Dipole moments of PBESOL GM for $n = 4 - 18$.

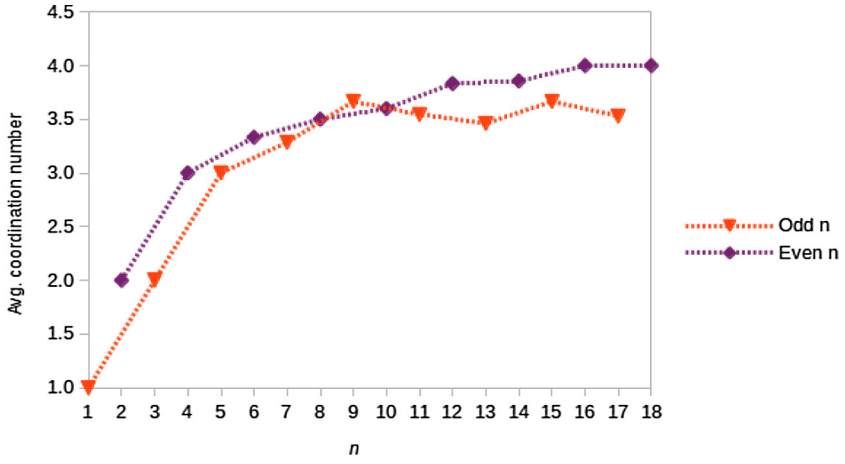


**Fig. 5.** Coordination numbers of PBESOL GM for $n = 1 - 18$; bond length cutoff ~2.95 Å.

As can be seen from the plot, the IP GM was found within very few iterations as indicated by the black line on the very bottom of the plot; the second-lowest energy structure, however, was only found after roughly 200 iterations, and since the relative energies of structures can change when they are re-evaluated using DFT, it is important to converge more than just the GM in this initial stage, and important to run for enough iterations to explore all key regions of the potential energy landscape. This behaviour is representative of EA convergence of all larger clusters.

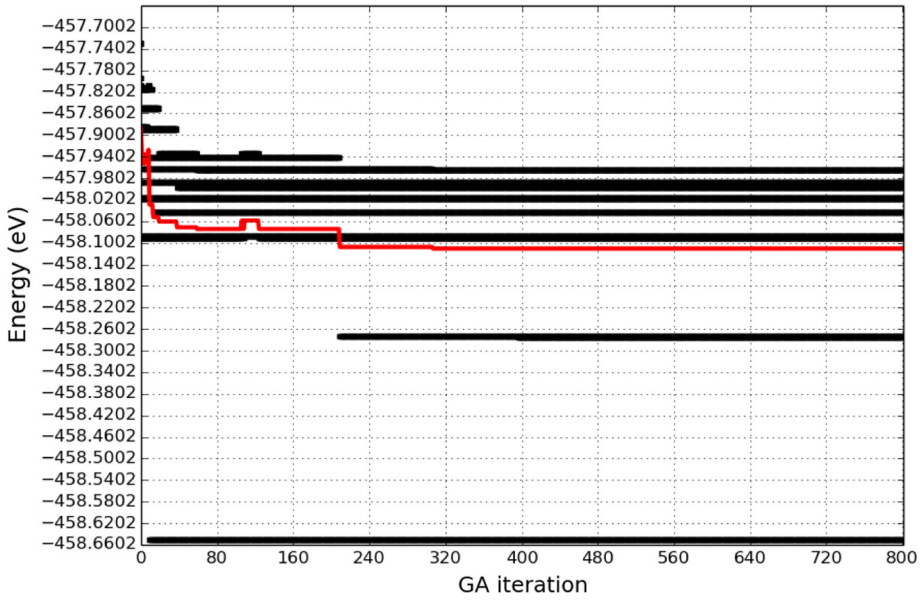


**Fig. 6.** Energy progression of the top 10 structures in each EA iteration. Black lines represent the top 10 individual structures that have been found in each EA generation, the red line is the average of these top 10 structures. (For interpretation of the references to colour in this figure legend, the reader is referred to the web version of this article.)

### 3.6. Comparison to other binary compounds

When comparing the results for barium oxide clusters to those for related compounds, the first choice is magnesium oxide; it is also an alkali earth oxide and several *ab initio* studies on structures of its nanoclusters have been published [5,26–28]. In particular, if $n$ is a multiple of 3 it has been found that barrel-like MgO structures are preferred over bulk-like structures for small nanoclusters with $n < 18$ [26]. Another study [29] showed that the preference for bulk-like over barrel-shaped clusters emerges in all alkali earth oxides with metals heavier than magnesium. For $n = 18$ and 24, studies have shown that MgO clusters also start adopting bulk-like structures [27]; the difference can therefore be described in terms of what size is necessary to achieve bulk cuts for the different alkali earth oxides.

Another compound which behaves much more like BaO at this scale is potassium fluoride. This is of particular interest as the ratio of ionic radii is 1:1 for both BaO and KF [30].

## 4. Conclusions

The atomic structures for barium oxide nanoclusters, based on density functional theory, of sizes up to $(BaO)_{24}$ were predicted. A manageable number of configurations that were refined in this study were generated by employing an evolutionary algorithm to search for the lowest energy local minima on the energy landscape - defined using an interatomic potential - for each size. It was found that global minima clusters with an even number of formula units resemble a cut from the rock salt phase, and such configurations were generally more stable. Further investigation into our results revealed that global minimum clusters with 8, 10 and 16 formula units were particularly more stable relative to both their neighbouring sized clusters and other local minima configurations of the same size. The latter make 8, 10 and 16, as well as sizes 4 and 6, magic size numbers. The latter implies that these configurations should make for the best targets to validate our computational results with experiment involving deposition of mass-selected clusters onto a substrate. A continuation of the work here on the computational side should involve inclusion of the substrate in calculations.

## 5. Notes

Structures reported in this paper will be uploaded to the WASP@N database [31].

All graphical representations of clusters were produced using VESTA [32].

## Acknowledgements

We are grateful to UCL for providing a DTA studentship and EPSRC for the WASP@N grant (Grant No. EP/I03014X). Via our membership of the UK's HEC Materials Chemistry Consortium, which is funded by EPSRC (Grant No. EP/L000202), this work used the ARCHER UK National Supercomputing Service (http://www.archer.ac.uk). We also wish to thank Dr. M. Farrow, Dr. A. Sokol and Prof. R. Palmer for helpful discussion.

## Appendix A. Supplementary material

Supplementary data associated with this article can be found, in the online version, at http://dx.doi.org/10.1016/j.comptc.2017.01.010.

## References

[1] D.J. Wales, H.A. Scheraga, Global optimization of clusters, crystals, and biomolecules, Science 285 (1999) 1368–1372.
[2] R.L. Johnston, Evolving better nanoparticles: genetic algorithms for optimising cluster geometries, Dalton Trans. (2003) 4193–4207.
[3] S. Heiles, R.L. Johnston, Global optimization of clusters using electronic structure methods, Int. J. Quantum Chem. 113 (2013) 2091–2109.
[4] S.M. Woodley, R. Catlow, Crystal structure prediction from first principles, Nat. Mater. 7 (2008) 937–946.
[5] M.R. Farrow, Y. Chow, S.M. Woodley, Structure prediction of nanoclusters; a direct or a pre-screened search on the DFT energy Landscape?, Phys Chem. Chem. Phys. 16 (2014) 21119–21134.
[6] S.M. Woodley, Knowledge led master code search for atomic and electronic structures of $LaF_3$ nanoclusters on hybrid rigid ionshell modeldft landscapes, J. Phys. Chem. C 117 (2013) 24003–24014.
[7] J.D. Gale, A.L. Rohl, The general utility lattice program (gulp), Mol. Simul. 29 (2003) 291–341.
[8] V. Blum, R. Gehrke, F. Hanke, P. Havu, V. Havu, X. Ren, K. Reuter, M. Scheffler, Ab initio molecular simulations with numeric atom-centered orbitals, Comput. Phys. Commun. 180 (2009) 2175–2196.

[9] J. Park, H. Elmlund, P. Ercius, J.M. Yuk, D.T. Limmer, Q. Chen, K. Kim, S.H. Han, D. A. Weitz, A. Zettl, A.P. Alivisatos, 3d structure of individual nanocrystals in solution by electron microscopy, Science 349 (2015) 290–295.
[10] K. Schouteden, K. Lauwaet, E. Janssens, G. Barcaro, A. Fortunelli, C. Van Haesendonck, P. Lievens, Probing the atomic structure of metallic nanoclusters with the tip of a scanning tunneling microscope, Nanoscale 6 (2014) 2170–2176.
[11] K.-J. Hu, S.R. Plant, P.R. Ellis, C.M. Brown, P.T. Bishop, R.E. Palmer, Atomic resolution observation of a size-dependent change in the ripening modes of mass-selected au nanoclusters involved in co oxidation, J. Am. Chem. Soc. 137 (2015) 15161–15168.
[12] Z.Y. Li, N.P. Young, M. Di Vece, S. Palomba, R.E. Palmer, A.L. Bleloch, B.C. Curley, R.L. Johnston, J. Jiang, J. Yuan, Three-dimensional atomic-scale structure of size-selected gold nanoclusters, Nature 451 (2008) 46–48.
[13] W. Gerlach, Die gitterstruktur der erdalkalioxyde, Zeitschrift für Physik 9 (1922) 184–192.
[14] R.A. Buckingham, The classical equation of state of gaseous helium, neon and argon, Proc. R. Soc. London A: Math. Phys. Eng. Sci. 168 (1938) 264–283.
[15] <http://www.ucl.ac.uk/klmc/potentials/> (accessed October 2015).
[16] G.V. Lewis, C.R.A. Catlow, Potential models for ionic oxides, J. Phys. C: Solid State Phys. 18 (1985) 1149.
[17] J.P. Perdew, K. Burke, M. Ernzerhof, Generalized gradient approximation made simple, Phys. Rev. Lett. 77 (1996) 3865–3868.
[18] J.P. Perdew, K. Burke, M. Ernzerhof, Generalized gradient approximation made simple [phys. rev. lett. 77, 3865 (1996)], Phys. Rev. Lett. 78 (1997), 1396–1396.
[19] J.P. Perdew, A. Ruzsinszky, G.I. Csonka, O.A. Vydrov, G.E. Scuseria, L.A. Constantin, X. Zhou, K. Burke, Restoring the density-gradient expansion for exchange in solids and surfaces, Phys. Rev. Lett. 100 (2008) 136406.
[20] C. Adamo, V. Barone, Toward reliable density functional methods without adjustable parameters: the pbe0 model, J. Chem. Phys. 110 (1999) 6158–6170.
[21] M.C.C. Wobbe, A. Kerridge, M.A. Zwijnenburg, Optical excitation of mgo nanoparticles; a computational perspective, Phys. Chem. Chem. Phys. 16 (2014) 22052–22061.
[22] A. Burnin, J. BelBruno, Znnsm+ cluster production by laser ablation, J. Chem. Phys. Lett. 362 (2002) 341.
[23] Y.J. Twu, C.W.S. Conover, Y.A. Yang, L.A. Bloomfield, Alkali-halide cluster ions produced by laser vaporization of solids, Phys. Rev. B 42 (1990) 5306–5316.
[24] J.P.K. Doye, D.J. Wales, Structural transitions and global minima of sodium chloride clusters, Phys. Rev. B 59 (1999) 2292–2300.
[25] <https://github.com/tomaslaz/klmc_analysis/blob/master/ga_energy_evolution.py> (accessed June 2016).
[26] R. Dong, X. Chen, X. Wang, W. Lu, Structural transition of hexagonal tube to rocksalt for (mgo)3n, 2n10, J. Chem. Phys. 129 (2008).
[27] Y. Zhang, H.S. Chen, B.X. Liu, C.R. Zhang, X.F. Li, Y.C. Wang, Melting of $(MgO)_n$ (n = 18, 21, and 24) clusters simulated by molecular dynamics, J. Chem. Phys. 132 (2010).
[28] K. Kwapien, M. Sierka, J. Dbler, J. Sauer, M. Haertelt, A. Fielicke, G. Meijer, Structural diversity and flexibility of mgo gas-phase clusters, Angew. Chem. Int. Ed. 50 (2011) 1716–1719.
[29] F. Bawa, I. Panas, Competing pathways for MgO, CaO, SrO and BaO nanocluster growth, Phys. Chem. Chem. Phys. 4 (2002) 103–108.
[30] R.D. Shannon, Revised effective ionic radii and systematic studies of interatomic distances in halides and chalcogenides, Acta Crystallographica Section A 32 (1976) 751–767.
[31] <https://hive.chem.ucl.ac.uk/> (accessed November 2016).
[32] K. Momma, F. Izumi, VESTA3 for three-dimensional visualization of crystal, volumetric and morphology data, J. Appl. Crystallogr. 44 (2011) 1272–1276.